THE JOURNAL OF PHYSICAL CHEMISTRY Letters

LETTER

pubs.acs.org/JPCL

Characterization of the Structure and Dynamics of the HDV Ribozyme in Different Stages Along the Reaction Path

Tai-Sung Lee,[†,‡] George M. Giambaşu,[†,‡] Michael E. Harris,[§] and Darrin M. York*[,†,‡]

[†]BioMaPS Institute and [‡]Department of Chemistry and Biological Chemistry, Rutgers University, Piscataway, New Jersey 08854, United States

[§]RNA Center and Department of Biochemistry, Case Western Reserve University School of Medicine, Cleveland, Ohio 44118, United States

Supporting Information

ABSTRACT: The structure and dynamics of the hepatitis delta virus ribozyme (HDVr) are studied using molecular dynamics simulations in several stages along its catalytic reaction path, including reactant, activated precursor, and transition-state mimic and product states, departing from an initial structure based on the C75U mutant crystal structure (PDB: 1VC7). Results of five 350 ns molecular dynamics simulations reveal a spontaneous rotation of U-1 that leads to an in-line conformation and supports the role of protonated C75 as the general acid in the transition state. Our results provide rationale for the interpretation of several important experimental results and make experimentally testable predictions regarding the roles of key active site residues that are not obvious from any available crystal structures.

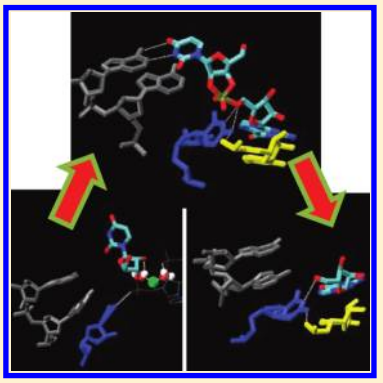

SECTION: Biophysical Chemistry

The hepatitis delta virus (HDV) ribozyme is a small catalytic RNA motif that is essential for viral replication during the HDV life cycle.[1−4] Recently, HDV-like ribozymes have been found to be widely distributed in nature, including in human genes, where they likely play a variety of important biological roles.[5] The HDV ribozyme (HDVr) catalysis reaction starts with an in-line nucleophilic attack of the U-1:$O_{2'}$ to the adjacent scissile phosphate, followed by cleavage of the P−$O_{5'}$ bond of G1 to produce a 2′,3′-cyclic phosphate and a 5′ hydroxy-terminus. Extensive structural and biochemical evidence suggests a catalytic mechanism involving acid−base catalysis; however, the detailed catalytic reaction mechanism of HDV ribozyme is still not resolved.

The first crystal structure of HDVr was reported in the product form[6] with an overall fold consistent with mutagenesis and chemical probing studies of the solution conformation.[7,8] In this product structure, C75:N_3 is in a position to form a hydrogen bond with G1:$O_{5'}$ (the leaving group); hence, it is reasonable to suggest that C75 acts as the general acid in phosphodiester bond cleavage reaction,[9,10] a hypothesis that is well supported by inactivation of the ribozyme by C75 mutation and a variety of experimental approaches.[9,11−13] Importantly, preactivation of the 5′O leaving group by substitution with a 5′S bridging phosphorothioate renders the ribozyme insensitive to C75 mutation.[10] Nevertheless, in the structures of the precleavage HDVr inactivated by C75U mutation and in the absence of Mg^{2+} ions, the active site has different arrangement in that U75 is posed to serve as the general base for cleavage reaction,[14] an interpretation that has been supported in certain molecular dynamics studies.[15−17]

Although not absolutely required for catalysis,[18] the presence of divalent metal ions at millimolar levels significantly enhances the HDVr reactivity.[2,3,7,19−21] It is believed that there is a hydrated Mg^{2+} ion near the active site.[9,14,22,23] This Mg^{2+} ion is likely to be involved in the HDVr catalytic reaction, as it has been shown that $Co(NH_3)_6^{3+}$ can compete with Mg^{2+} binding and inhibit HDVr activity.[9,24] The active site Mg^{2+} ion has been shown to interact directly with critical active site residues,[25,26] and modification of the linkage at the scissile phosphate can alter metal ion preference.[20,27]

Recently, Raman crystallographic experiments have determined that the pK_a value of C75 is shifted toward neutrality in a Mg^{2+}-dependent fashion[12] and furthermore that protonation of C75 may be coupled to changes in inner-sphere coordination of a divalent metal ion binding.[24,25] Subsequent crystallographic[28] and molecular dynamics[29,30] studies have provided new information about the HDVr active site, and, in particular, the nature of metal ion binding at a site involving a G·U wobble at the cleavage site and a rare reverse G·U wobble base pair located near the active site. Nonetheless, the conformational events that lead to a catalytically active state where U-1 is poised for in-line attack are not well understood because this residue was not resolved in the recent crystallographic study but rather modeled based on the conformation of the inhibitor strand of the hammerhead ribozyme. Furthermore, there has been relatively little reported work on the

Received: August 15, 2011
Accepted: September 19, 2011
Published: September 19, 2011

Table 1. Summary of Simulations Reported in the Present Work with Their Abbreviations Used in the Text[a]

abbrev	state	C75
RT-C75°-Mg	reactant	0
dRT-C75$^+$-Mg	activated precursor	+
ETS	early TS mimic	+
LTS	late TS mimic	+
Prod	product	0

[a] "TS" refers to "transition state" and "0" and "+" refer to neutral and protonated (at the N3 position) C75. Systems were solvated in a 60 × 60 × 120 Å^3 box of TIP3P waters[43] and an ion atmosphere corresponding to a 0.14 M bulk NaCl concentration, with residue C41 protonated. All simulations were carried out in the NPT ensemble at 1 atm and 298 K under periodic boundary conditions and using the smooth particle mesh Ewald method[44,45] for calculation of electrostatic interactions. For each system, 10 ns of water/ion equilibration, followed by an additional 10 ns of solute equilibration were performed, followed by 350 ns of production simulation, the last 300 ns of which was used for analysis. Simulations were performed with the NAMD simulation package (version 2.7b3)[46] using the AMBER[47,48] parm99 force field with the α/γ corrections for nucleic acids.[49]

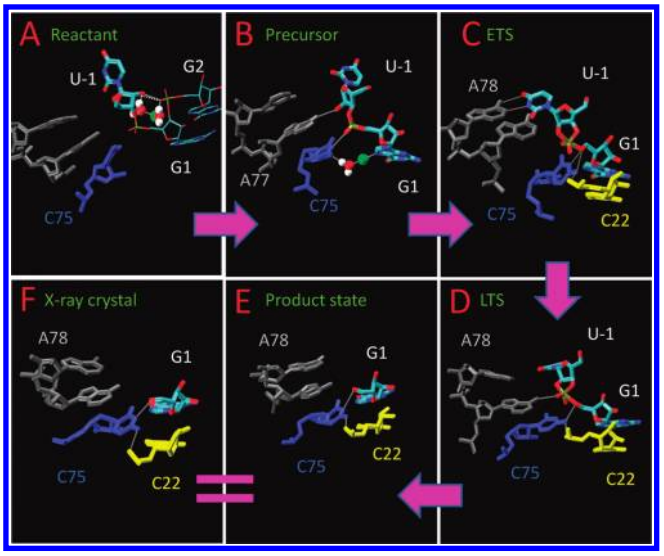

Figure 1. Graphic summary of the simulation results. Shown are representative snapshots from simulations listed in Table 1: (A) the neutral reactant state, (B) the precursor state with the nucleophile deprotonated and C75 protonated, (C) the early transition state mimic, (D) the late transition state mimic, (E) the product state, and (F) the crystal product structure (PDB ID: 1CX0).

HDVr structure and dynamics in different key stages along the catalytic reaction path.

The present study examines results from a series of molecular dynamics simulations of HDVr in different stages along the reaction path. Whereas previous simulation studies on HDVr focused on only the reactant states or the product state,[15,29−33] here we report results from a series of five 350 ns molecular dynamics simulations of HDV ribozyme (summarized in Table 1), the first focusing on different points along the reaction coordinates: (1) the reactant state (RT) with neutral C75 (C75°), (2) the activated precursor state with the nucleophile (U-1:$O_{2'}$) deprotonated (dRT) and C75 protonated (C75$^+$), (3) the early transition-state mimic (ETS), (4) the late transition-state mimic (LTS), and (5) the product state (Prod). The ETS and LTS transition-state mimics are formed by defining new chemical bonds between the nucleophile $O_{2'}$ and the active center P atom, with different bond lengths derived from high-level ab initio quantum calculations. The same protocol has been previously utilized in various simulation work of hammerhead ribozymes, where significant differences were observed in the ETS and LTS simulation results.[34,35] The unrefined starting structures were based on the 2.45 Å crystal structure of the C75U mutant (PDB: 1VC7),[14] which contains positions for the U-1 residue but that differs significantly from crystallographic data for the product structure[6] and from recent crystallographic data of HDVr bound to an inhibitor RNA containing a deoxynucleotide at the cleavage site.[28] In this structure, a metal ion is at the position between U75 and G25 and is directly coordinated to U75:O_4, which cannot occur in the wild type. Hence in our simulations the active Mg^{2+} ion was initially placed to be bound to G1:N_7, in accord with the position suggested by Chen et al.[26] In the first 10 ns of simulation, the Mg^{2+}−G1:N_7 distance was restrained to 2.0 Å. Initial simulations with the active-site metal ion placed at the original position of the C75U crystal structure indicated that with the native C75 the metal ion does not bind stably at this position. Recent crystallographic structure of the inhibited reactant[28] could be an alternative choice of the starting structure; however, the key nucleophile residue U-1 is missing in this structure and hence it was not selected here. The full details of the simulation protocol are provided in the Supporting Information.

The focus of this work is to present structure models in different stages of the HDVr reaction path. These simulation-derived models outline critical residues and their interactions, as shown in Figure 1. Different stages are shown: Figure 1A: the neutral reactant state (RT-C75°-Mg); Figure 1B: the precursor state with the nucleophile deprotonated and C75 protonated (dRT-C75$^+$-Mg); Figure 1C: the early transition state mimic (ETS); Figure 1D: the late transition state mimic (LTS); and Figure 1E: the product state (Prod). Statistical analyses were performed for the key geometry indexes, including bond distances, angles, dihedrals, and hydrogen bonds (H-bond). All indexes reported in the following sections were calculated from the last 300 ns out of the total 350 ns of trajectory for each simulation with a sampling rate of 100 ps. The hydrogen bonds are defined as formed when the distance between the donor and the acceptor is <3.5 Å and the angle is >150°. The H-bond is reported in terms of the percentage of the number of snapshots with formed hydrongen bonds compared with the total number of snapshots of each trajectory. The time series of mentioned H-bond distances are shown in Figure S1 of the Supporting Information.

In the neutral reactant state, G2:O_{2P} positions U-1:$O_{2'}$ for general base activation by the active site Mg^{2+} ion. Substitution of sulfur at the G2:O_{2P} position has a significant effect on HDVr activity that cannot be rescued by thiophilic metals,[36] and as yet, the origin of this effect remains unclear. In the RT-C75°-Mg simulation (Figure 1A), G2:O_{2P} forms a hydrogen bond with the U-1:$O_{2'}$ nucleophile (72% in a 300 ns trajectory). The interaction between G2:O_{2P} and U-1:$O_{2'}$ is further facilitated by a Mg^{2+}-mediated water bridge involving two inner sphere water molecules (Figure 1A).

The C75 position is held near the active site by the H-bond between C75:N_4 and the scissile phosphate G1:O_{2P} (45%). Therefore, C75 is not in a position near the leaving group to

act as a general acid, which is consistent with the precleavage crystal structure[14] and other simulation results.[15] However, the mechanisms cannot be unambiguously defined based on structural evidence corresponding to a single point along the reaction coordinate alone.[37] In this case, it is particularly precarious to assume that C75 does not act as the general acid, given the growing body of experimental evidence.[28] Furthermore, on the basis of its position in the precleavage state and the results from the RT-C75°-Mg simulation, rearrangement of active site interactions is needed for C75 to participate in this catalytic mode.

In the activated precursor state, A77, the active site Mg^{2+}, and C75, collectively hold the in-line conformation formed after a rigid rotation of U-1. A representative snapshot from the simulation of the activated precursor state with the nucleophile deprotonated and C75 protonated (dRT-C75$^+$-Mg) is shown in Figure 1B. During the simulations, the U-1 residue spontaneously undergoes a rigid rotation and reaches a near-in-line conformation around 20 ns, with the 2′O−P-5′O angle around 140°, rotates back to around 90° around 130 ns, and then rotates back to above 140° at around 200 ns. The in-line angle is kept around 140 degrees after 200 ns (average 138°, with maximum 162°). This observation shows that U-1 is able to adopt multiple conformations, consistent with recent crystallographic data of an inhibited precleavage structure where the electron density of U-1 was observed to be disordered.[28] After 200 ns, the in-line conformation of U-1 is stabilized by a new H-bond between A77:N_6 and the nucleophile (U-1:$O_{2'}$) (38%), between C75:N_3 and G1:O_{2P} (30%), and between C75:N_4 and G1:O_{2P} (56%). The A77:N_6/U-1:$O_{2'}$ H-bond interaction is intriguing in that it provides a rationale for the hitherto unexplained importance of the exocyclic NH_2 group of A77 identified through mutagenesis experiments.[38−40] The active site Mg^{2+} is directly bound to G1:N_7 (2.25 Å) and also bound to C75:$O_{2'}$ through a water molecule (5.20 Å). These interactions are consistent with experimental evidence, suggesting that a previously unobserved hydrated magnesium ion interacts with G1:N_7[26] as well as the observation that the reactivity of the HDVr is reduced 28 fold when C75 is mutated to deoxy-C75.[40]

In the early transition-state mimic simulation, U-1 forms a canonical WC pair with A78, and C75$^+$ forms strong H-bond with the leaving group. A dramatic change in the base pair hydrogen bonding occurs in the early transition-state mimic simulation, whereby a WC base pair forms between A78 and U-1 and is shown in Figure 1C. The occupancy of the H-bond between A78:N_6 and U-1:O_4 is 86%, whereas that between A78:N_1 and U-1:N_3 is 76%. This WC pair provides a rational for the importance of the identity of A78[38−40] as well as the nucleobase preference of the −1 position[32,41] and suggests that experiments involving correlated mutations in the 78 and −1 positions may provide further insight into the importance of this interaction, as it has been suggested that the U-1 preference can be altered under different conditions.[41]

In the ETS, the protonated C75$^+$ moves to a position where it is available to act as the general acid and is held in place by a strong H-bond between C75:N_4 (the exocyclic amine) and G1:$O_{O5'}$ (84%). At the same time, the exocyclic amine of C75 forms an additional hydrogen bonding interaction with C22:O_{2P} (57%), which helps to hold its position. The H-bond between C75:N_4 and C22:O_{2P} was observed crystallographically in the postcleavage structure[6] and in a recent precleavage structure[28] but not in the precleavage structure.[14] The exocyclic amine of C75 (N_4) thus appears to play an important role in maintaining the proper active site fold near the transition state, in agreement with conclusions from experiments that investigated the incorporation of 6-azauridine into the genomic HDV active site.[42]The Mg^{2+} loses its direct coordination with G1:N_7 and moves slightly away from the active site center when C75$^+$ moves toward G1:$O_{O5'}$, which is consistent with reported anticooperative binding of the Mg and C75 protonation.[26]

In the late transition state, the position of the general acid is maintained by H-bond interactions between A77:N_6 and G1:O_{2P} and C75:N_4 and C22:O_{2P}. In the late transition-state mimic, cleavage of the P−O5′ bond has progressed and there is an accumulation of negative charge at the G1:$O_{5'}$ position, leading to slight changes in the active site hydrogen bonding (Figure 1D). In the LTS, C75 has a similar position compared with the ETS, and the strong H-bond between C75:N_4 and G1:$O_{O5'}$ is maintained (65%). However, the WC pair between A78 and U-1, formed in the ETS is broken. Instead, because of the shift in the position of the reactive phosphate group, the exocyclic amine group of A77:N_6 now forms a strong H-bond with G1:O_{2P} (40%). The H-bond bond between C75:N_4 and C22:O_{2P} is more pronounced in LTS (86%) than in ETS (57%). The Mg^{2+} further loses both direct and indirect coordination interactions with G1:N_7 and C75:$O_{2'}$ and exits from the active site as the reaction proceeds to a late stage. This ejection of a metal from the HDV active site in the late stages of the reaction has been previously inferred from crystallographic data.[14]

In the product state, the Mg^{2+} exits the active site and the simulation converges toward the crystal structure of the product complex. In our simulation of the product state, A77 and A78 lose all H-bond interactions with the subtraction because U-1 no longer exists in the active site, as shown in Figure 1E. The H-bond between C75:N_3 and G1:$O_{O5'}$, reported in the postcleavage structure, is formed (56%) as well as the H-bond between C75:N_4 and C22:O_{2P} (43%). The strong H-bond between C75:N_4 and G1:$O_{O5'}$ observed in other stages no longer exists because C75 is now in its neutral state, having donated its proton to the $O_{5'}$ leaving group. Our simulation of the product state converges reasonably closely to that of the crystallographic data of the product structure,[6] with the exception of formation of a rare reverse G·U wobble base pair, also observed in a recent crystallographic structure of HDVr bound to an inhibitor RNA containing a deoxynucleotide at the cleavage site.[28] This reverse wobble may be further stabilized by divalent metal ion binding.

A key point is that our simulations of the product state were initiated not from the product crystallographic structure[6] but rather a precleavage structure of the C75U mutant.[14] Therefore, the observation that despite beginning with a distinct geometry along the reaction coordinate our simulations converge in both structure and hydrogen bonding pattern very closely to that of the postcleavage structure,[6] shown in Figures 1E,F and 2, provides an important internal check on reliability of our simulations.

The details of the catalytic mechanism of HDVr have been the topic of considerable discussion and debate, originating from varying mechanistic interpretations derived from crystallographic data and biochemical experiments. Of particular focus was the crystallographic structure of the C75U mutant in the precleavage state[14] that suggested the role of C75 as a general base rather than general acid, as was inferred by previous crystallographic data of the native product.[6] It was for this reason that we used this structure of the former as a departure point for our simulations of the native HDV at several stages along the reaction coordinate.

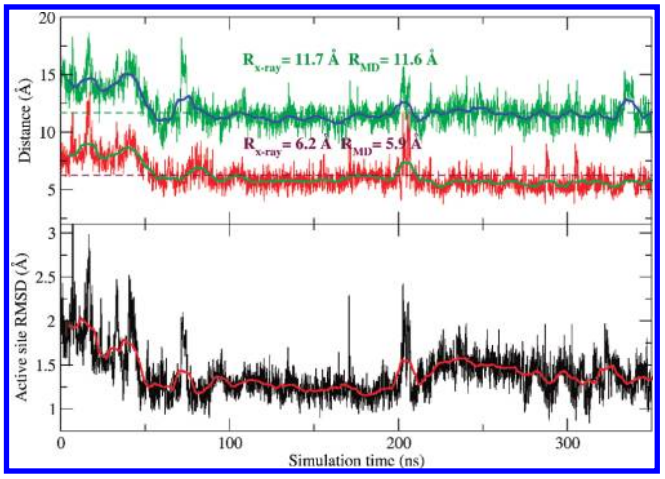

Figure 2. Product simulation converges toward the product (postcleavage) structure.[14] The upper plot shows two distances in the simulations versus the crystal distance: the first is the distance (in green) between A78:N_6 and G3:O_{2P}, whereas the second one is between A77:N_6 and G2:O_{2P}. R_{MD} refers to the average value from the simulations (from 50 to 350 ns). $R_{x\text{-}ray}$ refers to the distance in the crystal structure (PDB ID: 1CX0). The crystal structure distances are also plotted as dotted lines. The lower plot shows the active site rmsd of the product simulation with respect to the product crystal structure. The active site is defined as the collection of G1, G2, G3, C75, A77, and A78. Data are shown every 100 ps, and the smooth solid lines along the data curves are the window-averaged results with window size = 10.

Our results suggest that the position of C75, which is initially close to the U-1:$O_{2'}$ in the reactant state, prefers to adopt a hydrogen bonding interaction with the G1:O_{2P}, whereas the nucleophile interacts with G2:O_{2P} and a hydrated Mg^{2+} ion through a metal-mediated water bridge. These results do not support the role of C75 as that of a general base. Although the crystallographic structure of the C75U mutant was not in an in-line conformation required for nucleophilic attack, in the activated precursor simulation, U-1 reorients so as to form an in-line conformation that is stabilized by hydrogen bond interactions with A77.

The simulations of the transition state mimics indicate that protonated C75 adopts an orientation where it is poised to act as a general acid, acquiring interactions with the scissile phosphate and G1:$O_{5'}$ leaving group and being held in place, in part, by a hydrogen bond between the exocyclic amine of C75 and a nonbridge phosphoryl oxygen of C22 that supports a role for this functional group in maintaining the active site fold.[42] These changes in hydrogen bonding are accompanied by weakening and ejection of a divalent metal ion from the active site, consistent with crystallographic data.[14]

In the product state, the MD simulation results are observed to relax to within 1.5 Å rmsd from the product crystal structure, despite departing from a structure derived from the C75U precleavage structure. The only notable difference is that the simulations did not form a reverse G25·U20 wobble, as observed somewhat weakly in the product crystal structure[6] and more pronounced in a recent crystal structure of an inhibited reactant,[28] where G25 is in a syn conformation. This is not unexpected because the time scales of the simulations are likely not sufficient for G25 to flip from an anti conformation, seen in our simulations, to syn conformation to form a reverse wobble pair with U20.

Furthermore, on the basis of this inhibited reactant structure and MD simulations, an alternate metal binding site near the G25/U20 pair has been proposed,[28,29] where the G25·U20 reverse wobble base pair provides an environment for Mg^{2+} to bind to G25:N_7 and nearby active site residues. In our simulations, G25 is in the anti conformation and its N7 is not facing the active site hence G25:N7 cannot provide such binding environment.

In all of our simulations reported here (total >1.5 μs), no G25:U20 reverse wobble base pair has been observed, consistent with a previously reported MD studies.[15,31] Therefore, simulations with different G25 conformations may be needed to explore further the Mg^{2+} binding site near G25 and its relationship with the binding site we proposed in the present work. Experimentally, it would be of great interest to examine the HDVr activity with chemical modifications at the G25 position, including an N7 deaza modification to eliminate binding of Mg^{2+} to N7 or an 8-bromo substitution to favor the syn conformation required by the reverse wobble pair.

In conclusion, we present a set of extended molecular dynamics simulations for HDVr in different stages along the reaction path and characterize a conformational transition of U-1 into an in-line active conformation in the activated precursor state. Our simulations support the role of C75 as the general acid and identify several key residue interactions in different stages of the reaction. Our results provide explanations for the observed importance of several active site residues and suggest specific hypotheses that can be experimentally tested. Although simulations starting with other crystal structures may further explore different possible active site conformations, this work provides a departure point for further investigations into the catalytic chemical steps of the HDVr mechanism.

■ ASSOCIATED CONTENT

Supporting Information. Additional computational details. This material is available free of charge via the Internet at http://pubs.acs.org.

■ AUTHOR INFORMATION

Corresponding Author
*E-mail: york@biomaps.rutgers.edu.

■ ACKNOWLEDGMENT

We are grateful for financial support provided by the National Institutes of Health (GM62248 to D.Y.). Computational resources from The Minnesota Supercomputing Institute for Advanced Computational Research (MSI) were utilized in this work. This research was partially supported by the National Science Foundation through TeraGrid resources provided by Ranger at TACC and Kraken at NICS under grant number TG-CHE100072.

■ REFERENCES

(1) Kuo, M. Y.; Sharmeen, L.; Dinter-Gottlieb, G.; Taylor, J. Characterization of Self-Cleaving RNA Sequences on the Genome and Antigenome of Human Hepatitis Delta Virus. *J. Virol.* **1988**, *62*, 4439–4444.

(2) Sharmeen, L.; Kuo, M. Y.; Dinter-Gottlieb, G.; Taylor, J. Antigenomic RNA of Human Hepatitis Delta Virus Can Undergo Self-Cleavage. *J. Virol.* **1988**, *62*, 2674–2679.

(3) Wu, H.-N.; Lin, Y.-J.; Lin, F.-P.; Makino, S.; Chang, M.-F. Human Hepatitis ∂ Virus RNA Subfragments Contain an Autocleavage Activity. *Proc. Natl. Acad. Sci. U.S.A.* **1989**, *86*, 1831–1835.

(4) Lai, M. M. C. the Molecular Biology of Hepatitis Delta Virus. *Annu. Rev. Biochem.* **1995**, *64*, 259–286.

(5) Webb, C.-H. T.; Riccitelli, N. J.; Ruminski, D. J.; Luptak, A. Widespread Occurrence of Self-Cleaving Ribozymes. *Science* **2009**, *326*, 953.

(6) Adrian, R.; Ferré-D'Amaré; Zhou, K.; Doudna, J. A. Crystal Structure of a Hepatitis Delta Virus Ribozyme. *Nature* **1998**, *395*, 567–574.

(7) Perrotta, A. T.; Been, M. D. The Self-Cleaving Domain from the Genomic RNA of Hepatitis Delta Virus: Sequence Requirements and the Effects of Denaturant. *Nucleic Acids Res.* **1990**, *18*, 6821–6827.

(8) Wadkins, T. S.; Perrotta, A. T.; Ferre-D'Amare, A. R.; Doudna, J. A.; Been, M. D. A Nested Double Pseudoknot Is Required for Self-Cleavage Activity of Both the Genomic and Antigenomic Hepatitis Delta Virus Ribozymes. *RNA* **1999**, *5*, 720–727.

(9) Nakano, S.; Chadalavada, D. M.; Bevilacqua, P. C. General Acid-Base Catalysis in the Mechanism of a Hepatitis Delta Virus Ribozyme. *Science* **2000**, *287*, 1493–1497.

(10) Das, S.; Piccirilli, J. General Acid Catalysis by the Hepatitis Delta Virus Ribozyme. *Nature Chem. Biol.* **2005**, *1*, 45–52.

(11) Oyelere, A. K.; Kardon, J. R.; Strodel, S. A. pKa Perturbation in Genomic Hepatitis Delta Virus Ribozyme Catalysis Evidenced by Nucleotide Analogue Interference Mapping. *Biochemistry* **2002**, *41*, 3667–3675.

(12) Gong, B.; Chen, J.-H.; Chase, E.; Chadalavada, D. M.; Yajima, R.; Golden, B. L.; Bevilacqua, P. C.; Carey, P. R. Direct Measurement of a pKa near Neutrality for the Catalytic Cytosine in the Genomic HDV Ribozyme Using Raman Crystallography. *J. Am. Chem. Soc.* **2007**, *129*, 13335–13342.

(13) Cerrone-Szakal, A. L.; Siegfried, N. A.; Bevilacqua, P. C. Mechanistic Characterization of the HDV Genomic Ribozyme: Solvent Isotope Effects and Proton Inventories in the Absence of Divalent Metal Ions Support C75 as the General Acid. *J. Am. Chem. Soc.* **2008**, *130*, 14504–14520.

(14) Ke, A.; Zhou, K.; Ding, F.; Cate, J. H. D.; Doudna, J. A. a Conformational Switch Controls Hepatitis Delta Virus Ribozyme Catalysis. *Nature* **2004**, *429*, 201–205.

(15) Krasovska, M. V.; Sefcikova, J.; Špačková, Nad's; Šponer, Jiří; Walter, N. G. Structural Dynamics of Precursor and Product of the RNA Enzyme from the Hepatitis Delta Virus As Revealed by Molecular Dynamics Simulations. *J. Mol. Biol.* **2005**, *351*, 731–748.

(16) Banáš, P.; Rulíšek, L.; Hánošová, V.; Svozil, D.; Walter, N. G.; Šponer, J.; Otyepka, M. General Base Catalysis for Cleavage by the Active-Site Cytosine of the Hepatitis Delta Virus Ribozyme: QM/MM Calculations Establish Chemical Feasibility. *J. Phys. Chem. B* **2008**, *112*, 11177–11187.

(17) Banás, P.; Jurecka, P.; Walter, N. G.; Sponer, J.; Otyepka, M. Theoretical Studies of RNA Catalysis: Hybrid QM/MM Methods and Their Comparison with MD and QM. *Methods* **2009**, *49*, 202–216.

(18) Fedoruk-Wyszomirska, A.; Giel-Pietraszuk, M.; Wyszko, E.; Szymański, M.; Ciesiołka, J.; Barciszewska, M. Z.; Barciszewski, J. The Mechanism of Acidic Hydrolysis of Esters Explains the HDV Ribozyme Activity. *Mol. Biol. Rep.* **2009**, *36*, 1647–1650.

(19) Suh, Y. A.; Kumar, P. K.; Taira, K.; Nishikawa, S. Self-Cleavage Activity of the Genomic HDV Ribozyme in the Presence of Various Divalent Metal Ions. *Nucleic Acids Res.* **1993**, *21*, 3277–3280.

(20) Shih, I.-h.; Been, M. D. Ribozyme Cleavage of a 2′,5′-Phosphodiester Linkage: Mechanism and a Restricted Divalent Metal-Ion Requirement. *RNA* **1999**, *5*, 1140–1148.

(21) Shih, I.-h.; Been, M. D. Catalytic Strategies of the Hepatitis Delta Virus Ribozymes. *Annu. Rev. Biochem.* **2002**, *71*, 887–917.

(22) Bevilacqua, P. C.; Yajima, R. Nucleobase Catalysis in Ribozyme Mechanism. *Curr. Opin. Chem. Biol* **2006**, *10*, 455–464.

(23) Nakano, S.-i.; Bevilacqua, P. C. Mechanistic Characterization of the HDV Genomic Ribozyme: A Mutant of the C41 Motif Provides Insight into the Positioning and Thermodynamic Linkage of Metal Ions and Protons. *Biochemistry* **2007**, *46*, 3001–3012.

(24) Gong, B.; Chen, J.-H.; Bevilacqua, P. C.; Golden, B. L.; Carey, P. R. Competition Between Co(NH3)63+ and Inner Sphere Mg2+ Ions in the HDV Ribozyme. *Biochemistry* **2009**, *48*, 11961–11970.

(25) Gong, B.; Chen, Y.; Christian, E. L.; Chen, J.-H.; Chase, E.; Chadalavada, D. M.; Yajima, R.; Golden, B. L.; Bevilacqua, P. C.; Carey, P. R. Detection of Innersphere Interactions between Magnesium Hydrate and the Phosphate Backbone of the HDV Ribozyme Using Raman Crystallography. *J. Am. Chem. Soc.* **2008**, *130*, 9670–9672.

(26) Chen, J.-H.; Gong, B.; Bevilacqua, P. C.; Carey, P. R.; Golden, B. L. A Catalytic Metal Ion Interacts with the Cleavage Site GU Wobble in the HDV Ribozyme. *Biochemistry* **2009**, *48*, 1498–1507.

(27) Shih, I.-h.; Been, M. Kinetic Scheme for Intermolecular RNA Cleavage by a Ribozyme Derived from Hepatitis Delta Virus RNA. *Biochemistry* **2000**, *39*, 9055–9066.

(28) Chen, J.-H.; Yajima, R.; Chadalavada, D. M.; Chase, E.; Bevilacqua, P. C.; Golden, B. L. A 1.9 A Crystal Structure of the HDV Ribozyme Precleavage Suggests Both Lewis Acid and General Acid Mechanisms Contribute to Phosphodiester Cleavage. *Biochemistry* **2010**, *49*, 6508–6518.

(29) Veeraraghavan, N.; Ganguly, A.; Chen, J.-H.; Bevilacqua, P. C.; Hammes-Schiffer, S.; Golden, B. L. Metal Binding Motif in the Active Site of the HDV Ribozyme Binds Divalent and Monovalent Ions. *Biochemistry* **2011**, *50*, 2672–2682.

(30) Veeraraghavan, N.; Ganguly, A.; Golden, B. L.; Bevilacqua, P. C.; Hammes-Schiffer, S. Mechanistic Strategies in the HDV Ribozyme: Chelated and Diffuse Metal Ion Interactions and Active Site Protonation. *J. Phys. Chem. B* **2011**, *115*, 8346–8357.

(31) Krasovska, M. V.; Sefcikova, J.; Réblová, K.; Schneider, B.; Nils, G; Walter, J. S. Cations and Hydration in Catalytic RNA: Molecular Dynamics of the Hepatitis Delta Virus Ribozyme. *Biophys. J.* **2006**, *91*, 626–638.

(32) Sefcikova, J.; Krasovska, M. V.; Šponer, J.; Walter, N. G. The Genomic HDV Ribozyme Utilizes a Previously Unnoticed U-Turn Motif to Accomplish Fast Site-Specific Catalysis. *Nucleic Acids Res.* **2007**, *35*, 1933–1946.

(33) Veeraraghavan, N.; Bevilacqua, P. C.; Hammes-Schiffer, S. Long-Distance Communication in the HDV Ribozyme: Insights from Molecular Dynamics and Experiments. *J. Mol. Biol.* **2010**, *402*, 278–291.

(34) Lee, T.-S.; Silva-Lopez, C.; Martick, M.; Scott, W. G.; York, D. M. Insight into the Role of Mg^{2+} in Hammerhead Ribozyme Catalysis from X-ray Crystallography and Molecular Dynamics Simulation *J. Chem. Theory Comput.* **2007**, *3*, 325–327.

(35) Lee, T.-S.; Silva Lopez, C.; Giambaşu, G. M.; Martick, M.; Scott, W. G.; York, D. M. Role of Mg^{2+} in Hammerhead Ribozyme Catalysis from Molecular Simulation. *J. Am. Chem. Soc.* **2008**, *130*, 3053–3064.

(36) Jeoung, Y. H.; Kumar, P. K.; Suh, Y. A.; Taira, K.; Nishikawa, S. Identification of Phosphate Oxygens That Are Important for Self-Cleavage Activity of the HDV Ribozyme by Phosphorothioate Substitution Interference analysis. *Nucleic Acids Res.* **1994**, *22*, 3722–3727.

(37) Lee, T.-S.; York, D. M. Computational Mutagenesis Studies of Hammerhead Ribozyme Catalysis. *J. Am. Chem. Soc.* **2010**, *132*, 13505–13518.

(38) Kumar, P. K.; Suh, Y. A.; Miyashiro, H.; Nishikawa, F.; Kawakami, J.; Taira, K.; Nishikawa, S. Random Mutations to Evaluate the Role of Bases at Two Important Singlestranded Regions of Genomic HDV Ribozyme. *Nucleic Acids Res.* **1992**, *20*, 3919–3924.

(39) Wu, H. N.; Huang, Z. S. Mutagenesis Analysis of the Self-Cleavage Domain of Hepatitis Delta Virus Antigenomic RNA. *Nucleic Acids Res.* **1992**, *20*, 5937–5941.

(40) Nishikawa, F.; Shirai, M.; Nishikawa, S. Site-Specific Modification of Functional Groups in Genomic Hepatitis Delta Virus (HDV) Ribozyme. *Eur. J. Biochem.* **2002**, *269*, 5792–5803.

(41) Shih, I.-h.; Been, M. D. Energetic Contribution of Non-Essential 5′ Sequence to Catalysis in a Hepatitis Delta Virus Ribozyme. *EMBO J.* **2001**, *20*, 4884–4891.

(42) Oyelere, A. K.; Strobel, S. A. Site Specific Incorporation of 6-Azauridine into the Genomic HDV Ribozyme Active Site. *Nucleosides Nucleotides Nucleic Acids* **2001**, *20*, 1851–1858.

(43) Jorgensen, W. L.; Chandrasekhar, J.; Madura, J. D.; Impey, R. W.; Klein, M. L. Comparison of Simple Potential Functions for Simulating Liquid Water. *J. Chem. Phys.* **1983**, *79*, 926–935.

(44) Essmann, U.; Perera, L.; Berkowitz, M. L.; Darden, T.; Hsing, L.; Pedersen, L. G. A Smooth Particle Mesh Ewald Method. *J. Chem. Phys.* **1995**, *103*, 8577–8593.

(45) Sagui, C.; Darden, T. A. Molecular Dynamics Simulations of Biomolecules: Long-Range Electrostatic Effects. *Annu. Rev. Biophys. Biomol. Struct.* **1999**, *28*, 155–179.

(46) Phillips, J. C.; Braun, R.; Wang, W.; Gumbart, J.; Tajkhorshid, E.; Villa, E.; Chipot, C.; Skeel, R. D.; Kaleé, L.; Schulten, K. Scalable Molecular Dynamics with NAMD. *J. Comput. Chem.* **2005**, *26*, 1781–1802.

(47) Case, D. A.; Pearlman, D. A.; Caldweel, J. W.; Cheatham, T., III; Wang, J.; Ross, W. S.; Simmerling, C. L.; Darden, T. A.; Merz, K. M.; Stanton, R. V.; et al. *AMBER 7*; University of California, San Francisco: San Francisco, 2002.

(48) Pearlman, D. A.; Case, D. A.; Caldwell, J. W.; Ross, W. R.; Cheatham, T., III; DeBolt, S.; Ferguson, D.; Seibel, G.; Kollman, P. AMBER, a Package of Computer Programs for Applying Molecular Mechanics, Normal Mode Analysis, Molecular Dynamics and Free Energy Calculations to Simulate the Structure and Energetic Properties of Molecules. *Comput. Phys. Commun.* **1995**, *91*, 1–41.

(49) Pérez, A.; Márchan, I.; Svozil, D.; Sponer, J.; Cheatham, T. E., III; Laughton, C. A.; Orozco, M. Refinement of the AMBER Force Field for Nucleic Acids:Improving the Description of a α/γ Conformers. *Biophys. J.* **2007**, *92*, 3817–3829 .